Proceedings of the 12th International Conference on Fluid Flow, Heat and Mass Transfer (FFHMT 2025)
July 15, 2025 - July 17, 2025 | Imperial College London Conference, London, United Kingdom
Paper No. 239
DOI: 10.11159/ffhmt25.239

Form and Friction Drag Coefficients of Fine Screens: Streamlined and Rectangular Bar Profiles

Cumhur Ozbey[1], Serhat Kucukali[2]
[1]Hacettepe University, Civil Engineering Department, Hydraulics Division,
Ankara, Turkey
cumhurozbey@hacettepe.edu.tr; kucukali78@gmail.com

Abstract **-** Two different bar geometries of the fine screens used at the water intakes of hydropower plants, namely the streamlined Oppermann profile and the conventional rectangular profile, were numerically investigated to determine the corresponding form and friction drag coefficients. For both bar profiles, the bar thickness and the total bar length were s = 0.006 m and L = 0.083 m, respectively. FLOW-3D software was used to perform the simulations, where the Large Eddy Simulation (LES) was applied with a uniform mesh size of 0.001 m. Three different bar spacings of 4, 6, and 10 mm were tested under eight different approach velocities corresponding to bar Reynolds number and Reynolds number defined for bar length ranges of $300<Re_b<2400$ and $4150<Re_L<33200$, respectively. It was revealed that both form and friction drag coefficients are highly dependent on the shape of the bar. Accordingly, the average form drag coefficients for the Oppermann and rectangular bar profiles were found to be 1.20 and 3.23, respectively. Similarly, the average friction drag coefficients were obtained as 0.31 and 0.57, respectively. Also, for both bar geometries, it was shown that the form drag coefficient decreased until a certain limit of around Re_b=103 and remained almost constant despite the ongoing increase in the bar Reynolds number. However, as the Re_L increased, we observed a continuous reduction in the friction drag coefficient, which aligns with the analytical solutions. Moreover, both bar profiles yielded significantly higher form drag coefficients for narrower bar spacing. This result points out a strong correlation between the form drag coefficient and the head losses generated by fine screens at water intakes. Numerical analysis revealed that the form drag accounts for approximately 80% of the total drag, significantly contributing to the head losses at fine screens.

***Keywords*:** Fine Screen, Form Drag, Friction Drag, Numerical Modeling, Head Loss.

1. Introduction

The total drag coefficient of an object moving inside a fluid depends both on the shape and velocity of the object, and it is empirically defined as follows [1]:

$$C_d = \frac{2F_d}{\rho\, V^2 A} \tag{1}$$

where C_d – total drag coefficient [-], F_d – total drag force [N], ρ – fluid density [kg/m^3], V – flow velocity [m/s], A – projected frontal area of the body [m^2]. The drag force is a resistive force due to the stress distributions over the surface of the body, and it can be expressed in terms of the contribution of two different drag terms, namely the form and friction drag. The form drag, C_p, is the portion of the total drag force generated by the pressure distribution, whereas the friction drag, C_f, is created by the shear stress distribution. Thus, the total drag force exerted on a body can be written as:

$$C_d = C_p + C_f \tag{2}$$

For the fine screens that are used at the water intakes of hydropower plants, the bar Reynolds number can be expressed considering the bar thickness:

.

$$Re_b = \frac{Vs}{\nu} \tag{3}$$

where Re_b – bar Reynolds number [-], s – thickness of the bar [m], ν – kinematic viscosity of the fluid [m^2/s]. Similarly, the Reynolds number is defined based on the bar length as follows:

$$Re_L = \frac{VL}{\nu} \tag{4}$$

where Re_L – Reynolds number defined for bar length [-], s – total bar length [m]. In this present study, the form and friction drag coefficients are numerically determined and compared for the Oppermann and rectangular bar profiles. The details for the 3D bar profile of the Oppermann fine screen are given in [2]. The previous studies (e.g., [3]) on the screen head losses did not take into account the Reynolds number defined for the bar length. Thus, the objective of this study is to investigate the form and friction drag coefficients for the Oppermann and rectangular bar profiles in a numerical model for different bar spacings with the function of screen-related Reynolds numbers.

2. CFD Modeling

The computational fluid dynamics (CFD) models have recently emerged as a powerful tool for accurately predicting the complex behaviors of fluid flows [4, 5]. Accordingly, the numerical simulations were carried out in FLOW-3D software, which is a commercially available CFD package for simulating numerous types of flows by applying the finite volume method [5]. Free surfaces are modeled with one of the distinctive features of the software, namely the Volume of Fluid (VOF) approach, which enables three primary functions for free surface flows: (i) detecting the position and orientation of free surfaces within the computational cells, (ii) tracking the movements of the free surface through the cells, and (iii) employing a boundary condition at the interface of the free surface [6]. Hence, this VOF method allows for more accurate capturing of flow depths, resulting in improved predictions of head losses.

Within this context, the form and friction drag coefficients were numerically obtained for the Oppermann and rectangular bar profiles under the same initial and boundary conditions. Three different bar spacings of b = 4, 6, and 10 mm were tested under Re_b and Re_L ranges of 300–2400 and 4150–33200, respectively. Also, the bar thickness and total bar length for both bar geometries were kept constant at 0.006 m and 0.083 m, respectively.

2.1. Model Setup Establishment

Figure 1 shows the three-dimensional CFD model for the Oppermann profile, where the corresponding dimensions of the solution domain are given. The longitudinal direction is denoted by the x-axis, while the lateral and vertical directions are shown by the y- and z-axes, respectively. The length and width of the computational domain are 0.20 m and 0.05 m, respectively. The height of the mesh block is 0.22 m, where the water surface is defined at 0.20 m as an initial condition.

The boundary conditions are shown on the faces of the mesh block. Accordingly, a velocity boundary condition was applied at the inlet, while a pressure boundary condition, coupled with fluid elevation, was specified at the exit. For the sidewalls and the channel bottom, the symmetry and wall boundary conditions were set, respectively. Lastly, at the free surface, the atmospheric pressure was defined.

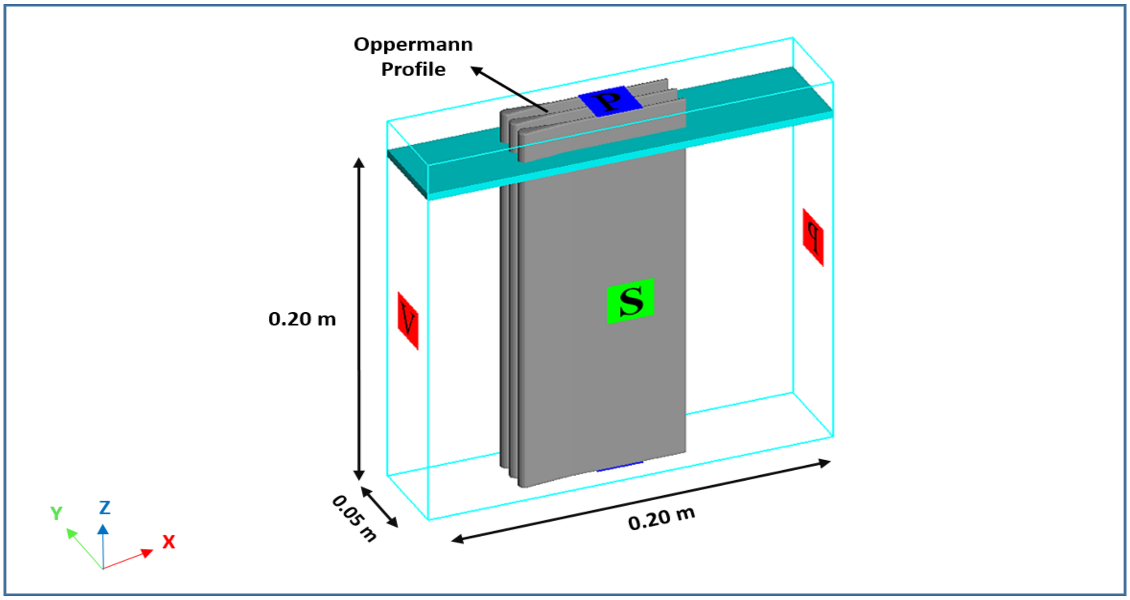

Fig. 1: The three-dimensional CFD model of the Oppermann profile with bar spacing of b = 4 mm. The entire solution domain is represented by a single mesh block where the boundary conditions are shown on each face. Accordingly, P = pressure, S = symmetry, and V = velocity.

2.2. Turbulence Model and Meshing

For the physics of the numerical model, the Large Eddy Simulation (LES) turbulence model was employed. The LES method has been used successfully by previous studies in order to solve a wide range of complex flow phenomena [7-11]. Unlike the Reynolds-averaged Navier-Stokes (RANS) turbulence models, where time-averaged solutions are obtained, the LES resolves the flow fields instantaneously, enabling more accurate and reliable results [12]. In this time-variant approach, the unsteady turbulent motions associated with large-scale structures are explicitly represented, while smaller-scale motions are modeled using the Smagorinsky model [13] as:

$$\tau_{ij} = -2v_t\bar{S}_{ij} \tag{5}$$

$$\bar{S}_{ij} = \frac{1}{2}\left(\frac{\partial \bar{u}_i}{\partial x_j} + \frac{\partial \bar{u}_j}{\partial x_i}\right) \tag{6}$$

where τ_{ij} stands for the anisotropic stress tensor, $\bar{S}_{ij}$ and $\bar{u}_i$ are the resolved rate of strain and resolved velocity field, respectively, v_t refers to the eddy viscosity and δ_{ij} is the Kronecker delta. For a wall-bounded flow, the normalized wall distance is defined as follows:

$$y^+ = u_* \, y/\nu \tag{7}$$

where u_* is the shear velocity, y refers to the absolute distance to the nearest wall, and ν is the kinematic viscosity of the fluid. Accordingly, for the given approach flow velocities in Table 2, the y^+ value for the first grid on each face of the computational domain was in the range of $1 < y^+ < 10$. The so-called range is consistent with the numerical study of [14].

Figure 2 illustrates how meshing was treated in the CFD model for all simulated cases. Considering the vicinity of the solid surfaces of both Oppermann and rectangular profiles and the near-wall region on the boundaries, a very fine grid was implemented to accurately resolve these regions. Accordingly, throughout all simulations, a structured grid size of 0.001 m was employed, where the cells were spatially uniform within the entire computational domain. Due to this very fine grid size, the Fractional Area/Volume Obstacle Representation (FAVOR) method in FLOW-3D is capable of incorporating the entire bar profile, including both leading and trailing edges, into the governing set of equations. Additionally, this mesh resolution is considered to be sufficient based on the LES study performed by [15]. In this regard, the total cells in the mesh block were different depending on the bar spacing (Table 1).

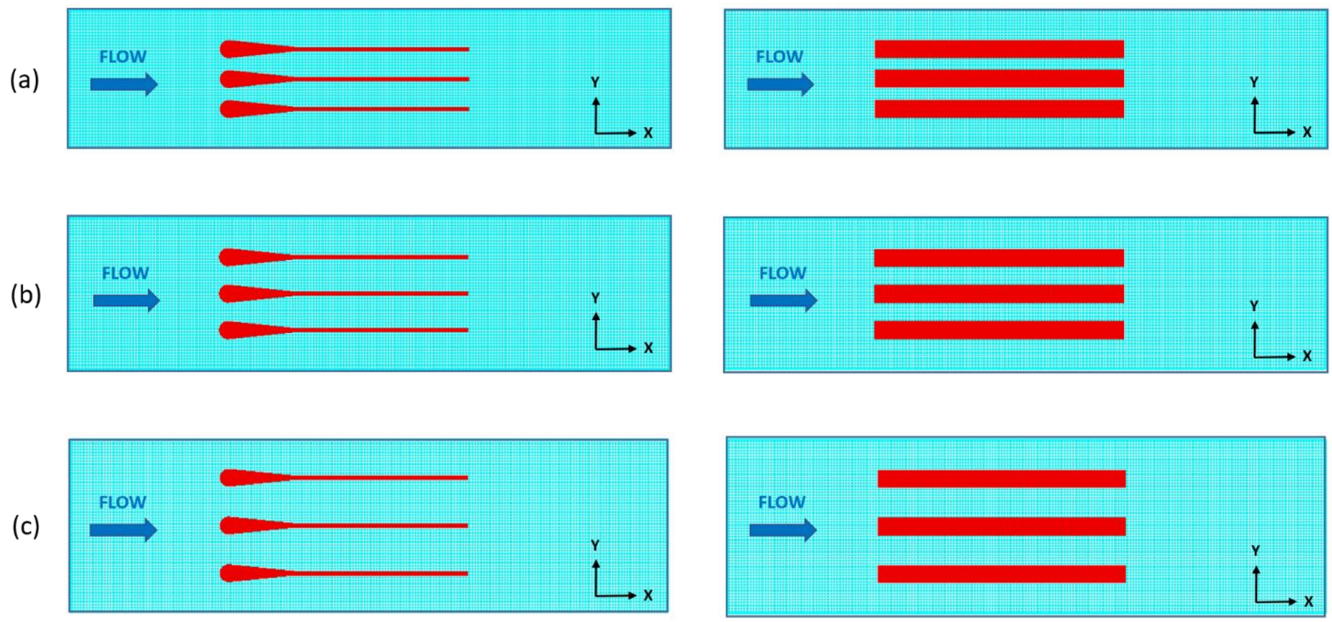

Fig. 2: Top view of the solution domain in the x-y plane for the Oppermann profiles on the left, and for the rectangular profiles on the right. (a) b=0.004 m, (b) b=0.006 m, and (c) b=0.010 m, where b represents the clear bar spacing. For all simulated cases, the grid size = 0.001 m, turbulence model = LES.

Table 1. Total number of cells employed in the CFD model for all simulated cases.

b (m)	Grid Size (m)	Total Cell Count	
		Oppermann Profile	Rectangular Profile
0.004	0.001	2.02×10^6	2.02×10^6
0.006	0.001	2.20×10^6	2.20×10^6
0.010	0.001	2.55×10^6	2.55×10^6

For all simulation runs, the initial time step was taken as 0.0001 sec, and the subsequent time steps were dynamically computed. Moreover, the first-order momentum advection scheme was employed throughout the simulations, and all simulations were run until the steady-state solution was reached.

3. Results and Discussion

Table 2 provides a summary of all simulation run conditions for the Oppermann and rectangular bar profiles, along with the corresponding form and friction drag, and the total drag coefficients for each tested case. Accordingly, the average form and friction drag coefficients for the Oppermann bar profile were numerically obtained as 1.20 and 0.31, respectively. On the other hand, for the rectangular profile, these values were found to be 3.23 and 0.57, respectively. Thus, it can be concluded that the form drag, on average, corresponds to approximately 80% of the total drag exerted on fine screens.

Table 2. All numerical test conditions and the form and friction drag coefficients of Oppermann and rectangular bar profiles.

				Oppermann Profile				**Rectangular Profile**			
b (m)	V (m/s)	Re_b (-)	Re_L (-)	C_p	C_f	C_d	C_p/C_f	C_p	C_f	C_d	C_p/C_f
0.004	0.05	300	4150	1.490	0.590	2.081	2.525	3.861	1.000	4.861	3.860
	0.10	600	8300	1.430	0.381	1.812	3.750	3.666	0.765	4.431	4.794
	0.15	900	12450	1.398	0.312	1.710	4.484	3.702	0.683	4.385	5.418
	0.20	1200	16600	1.385	0.275	1.660	5.029	3.700	0.628	4.327	5.893
	0.25	1500	20750	1.381	0.253	1.633	5.461	3.690	0.591	4.281	6.239
	0.30	1800	24900	1.377	0.238	1.614	5.791	3.831	0.569	4.397	6.732
	0.35	2100	29050	1.360	0.225	1.585	6.042	3.838	0.542	4.378	7.075
	0.40	2400	33200	1.369	0.218	1.587	6.284	3.783	0.514	4.295	7.354
0.006	0.05	300	4150	1.259	0.597	1.856	2.108	3.313	0.912	4.225	3.634
	0.10	600	8300	1.230	0.382	1.612	3.221	3.201	0.686	3.887	4.667
	0.15	900	12450	1.210	0.312	1.522	3.878	3.218	0.599	3.816	5.368
	0.20	1200	16600	1.204	0.277	1.481	4.352	3.212	0.548	3.759	5.858
	0.25	1500	20750	1.200	0.256	1.455	4.688	3.197	0.515	3.712	6.202
	0.30	1800	24900	1.196	0.241	1.437	4.968	3.337	0.497	3.831	6.714
	0.35	2100	29050	1.183	0.229	1.412	5.170	3.354	0.476	3.827	7.053
	0.40	2400	33200	1.180	0.221	1.401	5.348	3.346	0.454	3.798	7.364
0.010	0.05	300	4150	1.062	0.559	1.621	1.901	2.721	0.755	3.476	3.604
	0.10	600	8300	1.000	0.369	1.369	2.712	2.607	0.553	3.160	4.713
	0.15	900	12450	0.983	0.299	1.281	3.290	2.576	0.474	3.049	5.435
	0.20	1200	16600	0.985	0.268	1.252	3.678	2.590	0.435	3.024	5.949
	0.25	1500	20750	0.986	0.247	1.233	3.991	2.575	0.404	2.979	6.380
	0.30	1800	24900	0.984	0.232	1.217	4.236	2.628	0.394	3.022	6.675
	0.35	2100	29050	0.978	0.222	1.200	4.414	2.724	0.381	3.103	7.149
	0.40	2400	33200	0.969	0.216	1.185	4.487	2.740	0.367	3.105	7.465

*NOTE: b = bar spacing, V = approach flow velocity, Re_b = bar Reynolds number, Re_L = Reynolds number defined for bar length, C_p = form drag coefficient, C_L = friction drag coefficient, C_d = total drag coefficient.

In Figure 3, the form drag coefficients, C_p, of the Oppermann and the rectangular bar geometries are shown for three bar spacings of b=4, 6, and 10 mm, where the relevant parameter is the bar Reynolds number. The bar shape strongly influences the form drag coefficient, resulting in significantly higher values for the sharp-edged rectangular profile. Also, the form drag coefficient of the Oppermann bar profile was numerically found to decrease until around Re_b=103 and remain almost constant afterward. This result is also consistent with the existing experimental studies on streamlined bodies. Moreover, in all tested cases, the bar spacing of b=10 mm yielded the lowest form drag coefficients for both bar geometries. The correlation between form drag and head loss is evident in this result, as larger bar spacing and streamlined bar profiles of fine screens at water intakes lead to lower head losses.

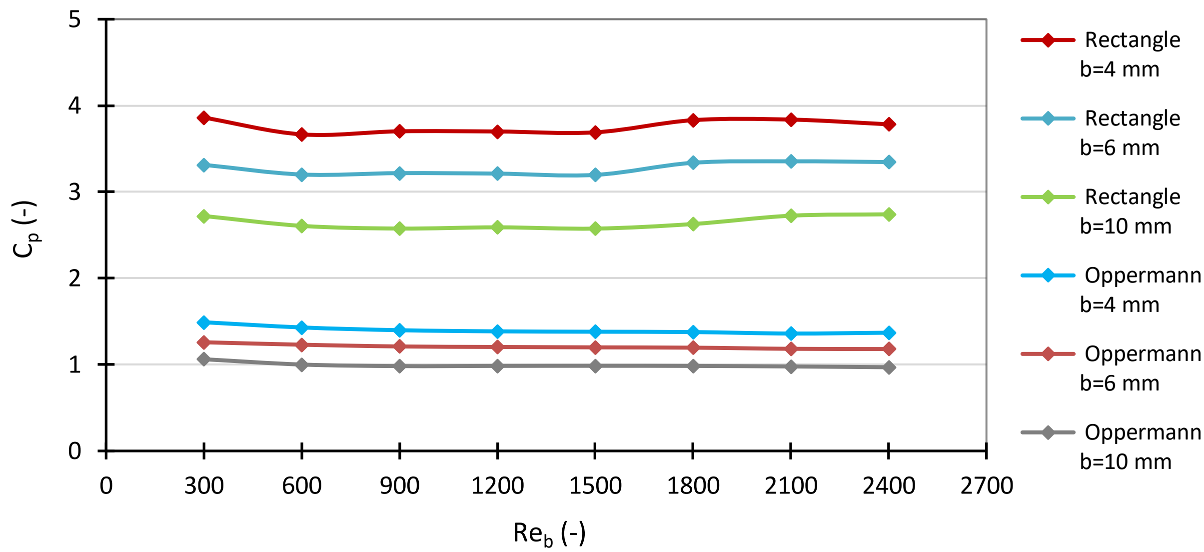

Fig. 3: Numerically obtained form drag coefficients with respect to the bar Reynolds number for the Oppermann and rectangular bar geometries. Turbulence model = LES, grid size = 0.001m, b = bar spacing, C_p = form drag coefficient, Re_b = bar Reynolds number.

Figure 4 shows how the friction drag coefficient, C_f, varies with the Re_L for both Oppermann and rectangular bar profiles across all simulated scenarios. Unlike the form drag coefficient, the friction drag coefficient consistently shows a decreasing tendency as the Re_L increases, irrespective of the bar profile.

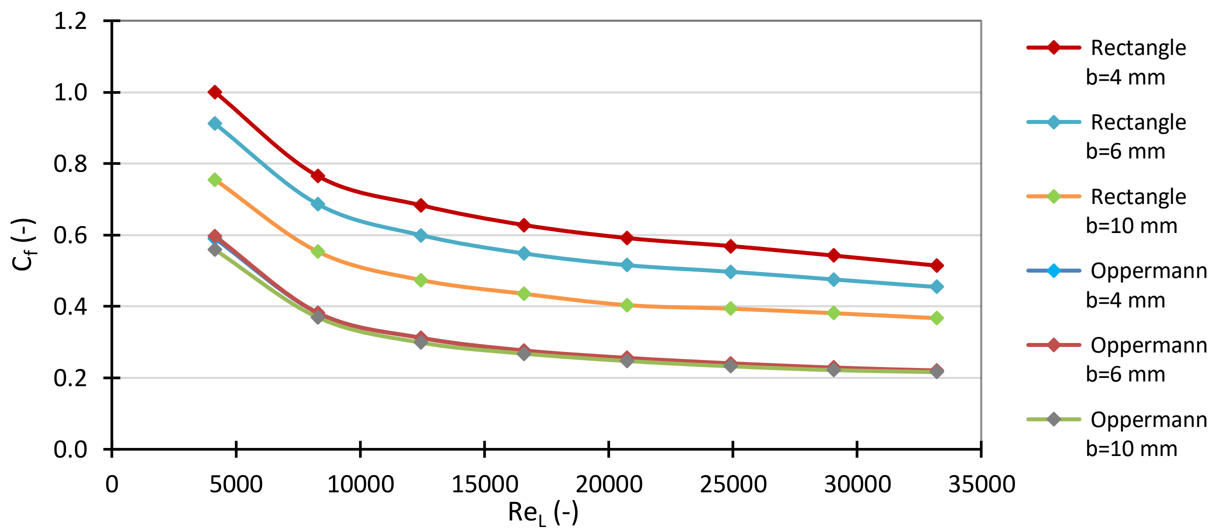

Fig. 4: Numerically obtained friction drag coefficients with respect to the Re_L for the Oppermann and rectangular bar geometries. Turbulence model = LES, grid size=0.001m, b=bar spacing, C_f = form drag coefficient, Re_L = Reynolds number defined for bar length.

For both tested bar geometries, Figure 5 shows the correlation between the form drag coefficient, C_p, and the experimentally obtained head loss coefficients. Accordingly, the coefficient of determination values were found to be R^2 = 0.95 and R^2 = 0.98 for the Oppermann and rectangular bar profiles, respectively. Thus, it can be concluded that the form drag coefficient strongly represents the head loss coefficients for the fine screens. However, further numerical analysis revealed that the friction drag coefficient, C_f, is very weakly correlated to the head loss coefficient, yielding R^2 = 0.001 and R^2 = 0.31 for the Oppermann and rectangular bar profiles, respectively.

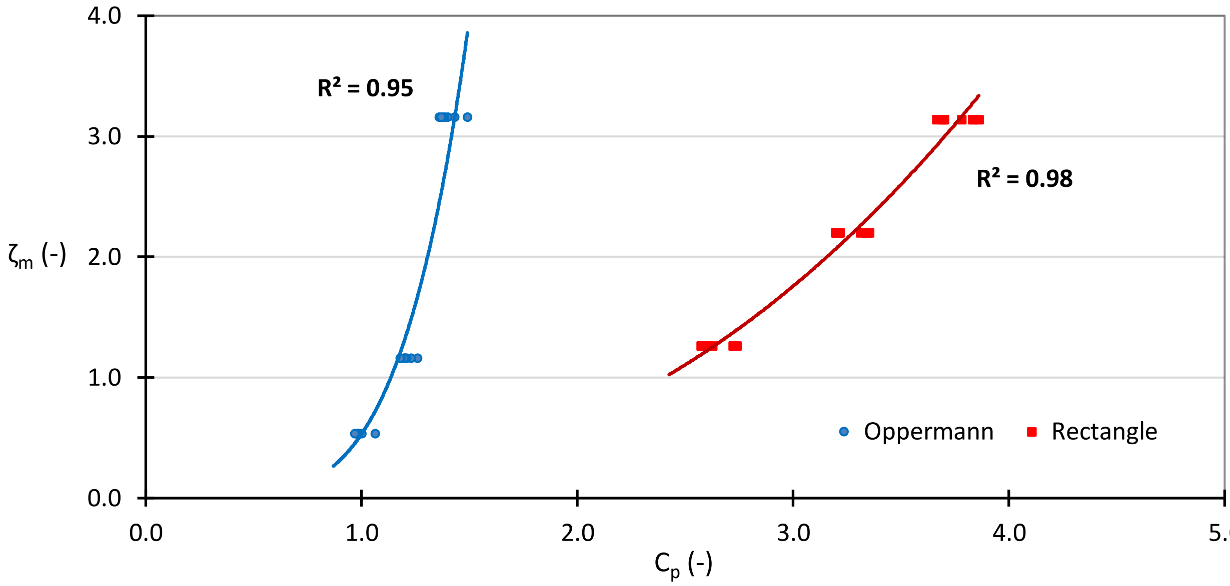

Fig. 5: Form drag coefficients, C_p, with respect to the measured head loss coefficients, ζ_m, for the Oppermann and rectangular bar profiles. The data source for bar spacing of b=4 mm and b=10 mm is [16], and the data source for bar spacing of b=6 mm is [17].

Depending on the measured head loss coefficients, the following power-law formulas are developed to correlate the form drag coefficient, C_p, to the head loss coefficients for the Oppermann and rectangular fine screens, respectively:

$$\xi_{\mathrm{opp}} = 0.53\, C_p{}^{4.96} \tag{8}$$

$$\xi_{\mathrm{rect}} = 0.11\, C_p{}^{2.54} \tag{9}$$

where ζ_{opp} – head loss coefficient for the Oppermann fine screen [-] and ζ_{rect} – head loss coefficient for the rectangular fine screen [-].

4. Conclusion

The form and friction drag coefficients for the Oppermann and rectangular bar profiles were numerically determined for different bar spacings under varying approach flow velocities. For the treatment of turbulence, the LES model was employed in all simulations where a structured grid size of 0.001 m was applied. The key findings of the present study can be summarized as follows:

- The streamlined Oppermann profile yielded much lower form drag compared to sharp-edged rectangular bar.
- The form drag was found to be around 80% of the total drag for both bar geometries.
- The numerical analyses suggested that the head loss coefficients can be reliably predicted from the form drag coefficient for the fine screens used at water intakes.
- Based on the experimental data, predictive equations for the head loss coefficient were proposed for both bar profiles.

Acknowledgements

This study is partially supported by Hacettepe University Scientific Research Project Program (BAP) grant with the agreement number FHD-2023-20760.

References

[1] H. Chanson, Applied Hydrodynamics, CRC Press, The Netherlands, 2014.
[2] C. Ozbey and S. Kucukali, "Numerical modeling of fish-friendly angled fine screens with porous media approach," in Proc. 10th Int. Symp. Hydraulic Structures, ETH Zurich, 2024, pp. 651–660.
[3] J. Meister, H. Fuchs, C. Beck, I. Albayrak, and R. M. Boes, "Head losses of horizontal bar racks as fish guidance structures," Water, vol. 12, p. 475, 2020.
[4] B. Andersson, R. Andersson, L. Håkansson, M. Mortensen, R. Sudiyo, and B. Van Wachem, Computational Fluid Dynamics for Engineers, Cambridge Univ. Press, 2012.
[5] J. Tu, G. H. Yeoh, C. Liu, and Y. Tao, Computational Fluid Dynamics: A Practical Approach, Elsevier, 2024.
[6] FLOW-3D, User Manual; Excellence in Flow Modelling Software, ver. 11.2, Flow Science, Inc., Santa Fe, NM, 2016.
[7] J. Bai, H. Fang, and T. Stoesser, "Transport and deposition of fine sediment in open channels with different aspect ratios," Earth Surf. Process. Landf., vol. 38, no. 6, pp. 591–600, 2013. doi: 10.1002/esp.3304.
[8] Y. Li, W. O. Wai, J. Zhan, W. Hu, and X.-F. Yan, "Evolution of three-dimensional flow field and vortex structures around a single spur dike during the scouring process," J. Hydraul. Eng., vol. 150, no. 1, p. 04023057, 2024. doi: 10.1061/JHEND8.HYENG-13617.
[9] Y. Liu, T. Stoesser, H. W. Fang, A. Papanicolaou, and A. G. Tsakiris, "Turbulent flow over an array of boulders placed on a rough, permeable bed," Comput. Fluids, vol. 158, pp. 120–132, Nov. 2017. doi: 10.1016/j.compfluid.2017.05.023.
[10] C. W. Zhao, H. W. Fang, Y. Liu, S. Dey, and G. J. He, "Impact of particle shape on saltating mode of bedload transport sheared by turbulent flow," J. Hydraul. Eng., vol. 146, no. 5, p. 04020034, 2020. doi: 10.1061/(ASCE)HY.1943-7900.0001735.
[11] C. W. Zhao, H. Fang, P. Ouro, T. Stoesser, and S. Dey, "Response of bedload and bedforms to near-bed flow structures," J. Hydraul. Eng., vol. 150, no. 1, p. 04023060, 2024. doi: 10.1061/JHEND8.HYENG-13618.
[12] S. B. Pope, Turbulent Flows, Cambridge: Cambridge Univ. Press, 2000.
[13] W. Rodi, G. Constantinescu, and T. Stoesser, Large-Eddy Simulation in Hydraulics, IAHR Monograph, CRC Press, The Netherlands, 2013.
[14] K. Miki and A. Ameri, "The effect of trailing edge grid resolution in large-eddy simulations," in Proc. Turbo Expo: Power for Land, Sea, and Air, vol. 87097, p. V13BT30A014, ASME, 2023.
[15] Z. Seifollahi Moghadam, F. Guibault, and A. Garon, "On the evaluation of mesh resolution for large-eddy simulation of internal flows using OpenFOAM," Fluids, vol. 6, no. 1, p. 24, 2021.
[16] H. C. Uysal, "Untersuchungen zur Hydraulik und zu den Verlusten von sehr feinen Fischschutzrechen," Diploma thesis, Faculty of Civil and Environmental Engineering, Univ. of Kassel, Germany, 2015. (in German)
[17] N. Schnell, "Fischschutz an Küstenschöpfwerken," Master's thesis, Univ. of Kassel, Germany, 2016. (in German)